2021 18th International Conference on Electrical Engineering, Computing Science and Automatic Control (CCE)
Mexico City, Mexico. November 10-12, 2021

Optoelectrothermoelectric properties of ternary chalcogenides thin films of $CuSbS_2$ and $Cu_{12}Sb_4S_{13}$

D. Trejo-Zamudio
Facultad de Química
UAQ
Santiago de Querétaro, Qro. México
daniel.trejo@uaq.edu.mx

S.A. Mayén-Hernández
Facultad de Química
UAQ
Santiago de Querétaro, Qro. México
sandra.mayen@uaq.edu.mx

J.G. Quiñones-Galván
Departamento de Física
UDG
Guadalajara, Jalisco, México
jose.quinones@academicos.udg.mx

F.J. de Moure-Flores
Facultad de Química
UAQ
Santiago de Queréretaro, Qro. México
fcomoure@hotmail.com

M.L. Gómez-Herrera
Facultad de Ingeniería
UAQ
Santiago de Queréretaro, Qro. México
lucero.gomez@uaq.mx

J. Santos-Cruz
Facultad de Química
UAQ
Santiago de Querétaro. Qro. México
jsantos@uaq.edu.mx

Abstract*—In this work, the preparation and study of two-phases as a thin film of $CuSbS_2$ and $Cu_{12}Sb_4S_{13}$ respectively is reported. These samples were obtained through a two-stage process: the sequential deposition of Sb_2S_3 and CuS, varying the thickness, on glass substrates and annealing at 350 °C in a nitrogen atmosphere. Subsequently, the films were characterized by Raman spectroscopy, ultraviolet-visible spectroscopy, EDS analysis, Hall effect and Seebeck coefficient. The objective was to study the properties of films for thermoelectric applications. The best sample was obtained with an initial thickness of 400 nm of Sb_2S_3 and 180 nm of CuS (ratio of 2.22). This sample, called CSS 2.22, shows some compounds rich in Cu. The band gap of the sample was 1.83 eV. Its charge carries concentration was $3.725x10^{22}$ cm^{-3} with a p-type conductivity. The conductivity value was $5.223x10^{2}$ $\Omega^{-1}cm^{-1}$ and the Seebeck coefficient was of 54.3 μV/K. Finally, the power factor value was 1.54 μW/cm·K at 60 °C.

Keywords*—$CuSbS_2$ chalcostebite, $Cu_{12}Sb_4S_{13}$ tetrahedrite, chalcogenide, thermoelectric material

I. INTRODUCTION

Currently there are technologies to produce heat, mechanical and electrical energy from renewable and clean energy sources, such as solar, wind, hydro, and bioenergy. However, the energy produced is no used 100 % and statistical results show that more than 60 % of this is wasted throughout the world, especially in form of heat [1].

One way to take advantage of this wasted energy in form of heat is using thermoelectric materials, which are materials with the capacity to convert heat into electricity. In turn, systems that use thermoelectric materials offer the advantages of being friendly to the environment, since they do not produce CO_2 emissions on site, they are small, can work in a wide temperature range, are reliable and have a long period of life [1], [2].

Currently there is a great variety of thermoelectric materials, there are materials based on metals, ceramics, polymers and semiconductors [2]. Metal-based materials have the advantage of having high electrical conductivities but high thermal conductivities as well, which translates into low efficiency. Remembering that the thermoelectric efficiency, *ZT,* is given by the equation:

$$ZT = \propto^2 \sigma T/K \qquad (1)$$

where $\propto$ is the Seebeck coefficient, sometimes denoted by *S,* σ is the electrical conductivity and *K* is the thermal conductivity [2].

In addition, many of them are made on basis of heavy metals such as Pb and Te, with the disadvantage of high toxicity and instability at high temperatures ($\sim$1000 K) [3]. New alternatives to these materials have been studied, such as the use of copper and sulfur materials. Cu-Sb-S based materials have some advantages such as the elements that compose it are abundant in the earth, are low-toxic and economics [4].

Some ternary compounds of copper, antimony and sulfur have been investigated for use in photovoltaic and some thermoelectric applications. Of these the $CuSbS_2$ and $Cu_{12}Sb_4S_{13}$ are of interest to obtain thin films by means of the Physical Vapor Deposition (PVD) technique. This type of deposit has been used to obtain these phases by means of sequential evaporation and using a subsequent annealing [4]. In the case of $CuSbS_2$, it has been studied more for photovoltaic applications [4], [5]. This compound is a semiconductor with a direct optical band gap of 1.4 to 1.6 eV, with a moderate hole density of 10^{15} to 10^{18} cm^{-3} [4], [6]–[8]. While tetrahedrite ($Cu_{12}Sb_4S_{13}$), it has been investigated to greater extent for thermoelectric applications given its complex structure and low thermal conductivity. In an investigation, thin films of this compound were obtained by the e-beam evaporation technique, with a reported band gap of $\sim$1.8 eV and a power factor ($S^2\sigma$) of up to 2.3 μW/cm-K^2 [9]. A high concentration of charge carriers of up to (10^{20} cm^{-3}) has been reported [10].

In this paper we report the synthesis of thin films by a sequential thermal evaporation of antimony and copper sulfide powders on glass substrates. This process was followed by annealing of the thin films in a nitrogen atmosphere. The samples obtained were characterized by Raman spectroscopy, ultraviolet-visible spectroscopy, EDS, Hall effect and Seebeck coefficient.

978-1-6654-0029-9/21/$31.00 ©2021 IEEE

II. METHODOLOGY

A. Preparation of thin films

Ternary chalcogenide films were obtained by a procedure similar to that described by Medina-Montes et al. [4]. The procedure consisted of two stages, the sequential deposit of sulfide films and the thermally annealed of the films in a N_2 atmosphere.

Glass substrates of 7.5 cm x 2.5 cm were used to the deposit of sulfides. The glass substrates were cleaned with soap, treated with chromic acid for 24 hours and subsequently attacked with nitric acid solution close to the boiling point for 3 hours.

In the first stage, using the physical evaporation deposit technique, a layer of antimony (III) sulfide (Sb_2S_3) followed by a layer of cooper (II) sulfide (CuS) were deposited on the substrates. Pure Sigma-Aldrich powders were used in this work. During the deposit of the sulfide layers, room temperature was maintained in the chamber and substrates. The vacuum pressure to start the grown was 6 x 10^{-5} mbar and the distance between the source to the substrate was 16 cm. The applied current for the antimony and copper sulfide was 120 and 210 A respectively. The antimony sulfide powders were first deposited on glass substrates under the pressure, distance and temperature conditions mentioned above. Subsequently, the vacuum inside the chamber was removed and the copper sulfide powders were placed on the current source. The copper sulfide was deposited on the antimony sulfide layer under the same conditions of temperature, distance, and pressure. Two glass substrates were used in each process. Finally, the sample obtained had a structure: glass substrate/Sb_2S_3/CuS.

The thickness of the Sb_2S_3 film used in this work was 400 nm and the thickness of the CuS film was varied by 100, 125, 175 and 180 nm. The thickness ratio between the Sb_2S_3 and CuS were 4.00, 3.20, 2.29 and 2.22. Each sample was labeled as CSS 4.00, CSS 3.20, CSS 2.29, and CSS 2.22 The thicknesses of the samples were measured by profilometry.

In the second stage, the samples were thermally annealed at 350 °C in a quartz tubular furnace of Lindberg Blue M., in atmosphere of N_2 gas for 2 hours. Table I summarizes the conditions in which the samples were obtained.

TABLE I. CONDITIONS FOR THE PREPARATION OF THE SAMPLES

Sample	Film thickness (nm)		Annealing temperature (°C)
	Sb_2S_3	CuS	
CSS 4.00	400	100	350
CSS 3.20	400	125	350
CSS 2.29	400	175	350
CSS 2.22	400	180	350

B. Characterization techniques

The thicknesses of the samples were measured with an Alpha-Step D-100 profilometer, KLA Tencor. Raman spectroscopy measurements were acquired with a Thermo Scientific DXR2 system equipped with a 633 nm laser as excitation source. The transmittance of films was measured using Genesys 10S UV-VIS, Thermo Scientific. The electric properties were measured using a Hall Effect Measurement System (ECOPIA HMS-300). Elemental composition of the samples was determined by energy dispersive spectroscopy, EDS analysis in a Hitachi SU1510. The Seebeck coefficient of the samples was measured using a system made up of Peltier devices and a Keithley 740 microvolmeter. Finally, the power factor was obtained by multiplying the electrical conductivity of the material by square of the Seebeck coefficient ($S^2\sigma$).

III. RESULTS AND DISCUSSION

A. Raman characterization

Fig. 1 shows the Raman spectra of the samples, where two vibrational modes were observed with marked centers at 335 y 358 cm^{-1}, attributable to $CuSbS_2$ and $Cu_{12}Sb_4S_{13}$ compounds respectively [4], [5], [11], [12]. The Raman band at 335 cm^{-1} is close to 329 cm^{-1} and belongs to the compound $CuSbS_2$, according to the literature [12]. On the other hand, the Raman band at 358 cm^{-1} is close to 355 cm^{-1} and is related with the tetrahedrite structure [4], [13]. In the Raman spectra of the CSS 2.22 and CSS 2.29 samples, it can be observed that both phases coexist. Likewise, it can be observed that in these two samples a slight signal is detected near 300 cm^{-1} that is attributed to unreacted Sb_2S_3, as has been reported in some studies [14]. The CSS 4.00 and CSS 3.20 samples present only a band with center at 335 cm^{-1}, which is due to the presence of $CuSbS_2$. No vibrational modes were found corresponding to secondary binary phase of CuS at 470 cm^{-1} as explained Medina-Montes et. al, which could indicate that there are no remains of this precursor in the samples [4]. From the Raman results it can be concluded that while the amount of copper sulfide increases and the annealing temperature is constant, the formation of tetrahedrite is favored; this is because stoichiometrically there is an excess of Cu and S.

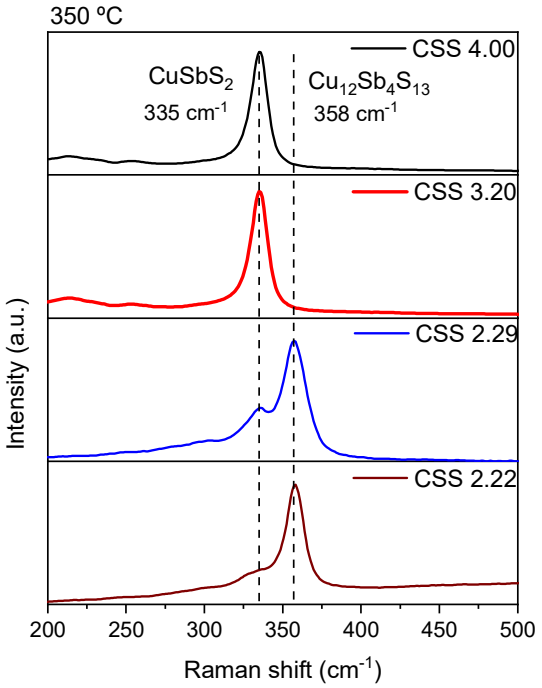

Fig. 1. Raman spectra of CSS samples.

According to Medina-Montes and collaborators, the Raman data in Fig. 1 can be used to quantify the number of phases contained in the sample, for this is necessary to exclude the part of Sb_2S_3 that did not react. Based on this, the following equation was employed:

$$Area_{Cu-Sb-S}(\%) = \frac{Area_{Cu-Sb-S}}{Area_{CuSbS_2} + Area_{Cu_{12}Sb_4S_{13}}} x100$$

Where $Area_{Cu-Sb-S}$ is the area of Raman band at either 335 cm^{-1} ($Area_{CuSbS_2}$) or 358 cm^{-1} ($Area_{Cu_{12}Sb_4S_{13}}$) [4].

Fig. 2 presents the results of the phase percentage estimation. The phase change can be observed when the amount of copper sulfide increases, this is due to the excess of Cu that favors the formation of tetrahedrite [15].

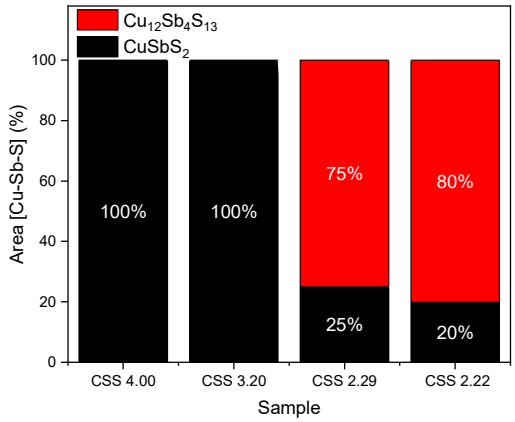

Fig. 2. Phases content in the CSS samples annealed at 350 °C.

These results are of interest since if there are large amounts of secondary phases, in this case $CuSbS_2$, it could affect the properties of the material, especially the Seebeck coefficient. Furthermore, the presence of secondary phases could favor the presence of grain boundaries or cracks that could affect the thermal and electrical conductivities of the material [16]. The results of the electrical conductivities and the Seebeck coefficient are presented later to determine the effect of the presence of a secondary phase.

B. Optical Characterization

Fig. 3 shows the transmittance spectra of the thin films obtained. The CSS 4.00 and CSS 3.20 samples have a similar spectrum with a transmittance edge near a wavelength of 735 nm and a maximum transmission near 65% for a wavelength of approximately 990 nm. These two samples are those that present the compound $CuSbS_2$ in Raman spectroscopy.

The CSS 2.29 sample has a transmittance edge close to the previous two samples, since it presents a combination of phases. The spectrum of the sample presented a lower transmittance and a change in the spectrum from 900 nm respect to the previous samples, which indicates the presence of two coexisting phases.

The CSS 2.22 sample has a different spectrum from the other samples, since by means of Raman spectroscopy it was found that is the sample with the highest amount of tetrahedrite (80%). It has an edge near the 600 nm wavelength and a transmittance below 15 %, in addition to being the sample with the greatest thickness.

Fig. 4 presents the direct optical band gap for the samples. For this, the Beer-Lambert law was used to calculate the absorbance and the absorption coefficient α. Subsequently, the band gap was estimated using the Tauc parabolic bands model. Fig. 4 shows the extrapolation of the linear region of $(\alpha hv)^2$ vs hv to the x-axis. For this, the thicknesses obtained by profilometry were 420, 440, 490 and 505 nm for the CSS 4.00, 3.20, 2.29 and 2.22 respectively. The CSS 4.00 and CSS 3.20 samples have a similar band gap of 1.71eV and 1.69 eV respectively, corresponding to $CuSbS_2$ similar to that reported in the literature of 1.4 to 1.6 eV[4], [6]–[8]. The CSS 2.29 sample has a band gap of 1.92 eV and was hardly to be identified because the sample has a combination of phases. Finally, the sample CSS 2.22 has a band gap value of 1.83 and it is a similar value obtained by e-beam technique [9]. This is because the sample has a higher percentage of $Cu_{12}Sb_4S_{13}$ and therefore the band gap tends towards the value of this phase when it is pure.

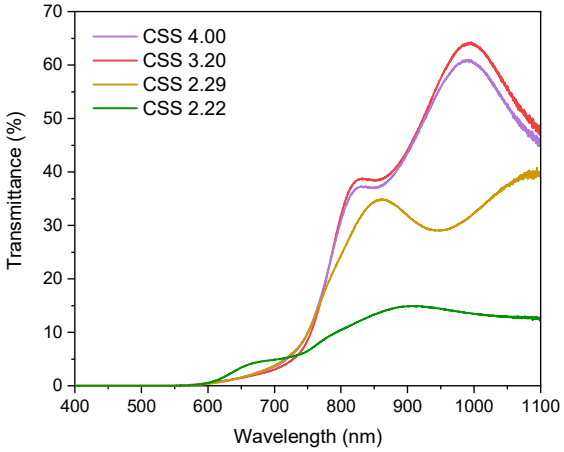

Fig. 3. Transmittance spectra of CSS samples.

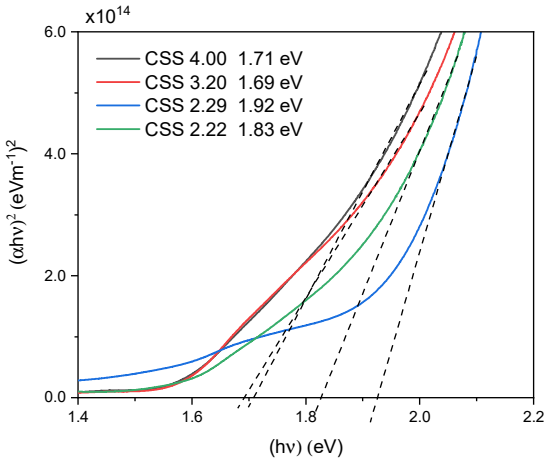

Fig. 4. Tauc plots of CuSbS films.

C. EDS analysis

Table II shows the elemental composition of the samples CSS annealed at 350 °C. The amounts in atomic percentage (at%) of Cu, Sb, S show a difference with the ideal composition of $CuSbS_2$ and $Cu_{12}S_4bS_{13}$. Only the CSS 2.22 sample has comparable results for tetrahedrite films obtained using the e-beam technique with an applied current of 40 mA, which showed mixing of some phases, especially CuS

and Cu_3SbS_4 [9]. The most notable difference is between the amount of Cu and S. In all samples, the amount of Cu is greater than what would ideally be expected, on the other hand the amount of S decreases. This is due to the variation in the thickness of CuS, where stoichiometrically there may be an excess of copper sulfide. Another explanation is that during annealing, sulfur evaporates, which generates deficiencies of this element in the samples and the amount of copper increases. In addition, the presence of secondary phases in the samples must be considered.

The best thickness ratio in other study to find the chalcostebite phase was 2.5 and annealed at 350 °C [4]; however, at close conditions in this investigation, ideal compositions were not obtained for any phase. Therefore, it is suggested to anneal in an atmosphere rich in sulfur that allows increasing the amount of this element, since the amounts of Sb are close to those that would be expected.

TABLE II. ELEMENTAL COMPOSITION OF CSS SAMPLES

Sample	(%) Atomic		
	Cu	Sb	S
CSS 4.00	36.16	22.15	41.70
CSS 3.20	37.97	20.51	41.53
CSS 2.29	51.99	13.05	34.96
CSS 2.22	50.54	11.49	37.97
$CuSbS_2$[a]	**25.0**	**25.0**	**50.0**
$Cu_{12}Sb_2S_{13}$[a]	**44.4**	**7.4**	**48.2**

[a]Ideal composition

D. Electrical characterization

Table III shows the results of the electrical measurements carried out using the Hall effect. Samples of 1 x1 cm were employed in the van der Pauw configuration. The results for chalcostebite, samples CSS 4.00 and CSS 3.20, are far from those reported in the literature. The concentration of charge carriers is lower to that reported (10^{15} to 10^{18} cm^{-3}) [4], [6]–[8]. This may be due to sulfur deficiency, remembering that the compound is p-type, its majority charge carries are holes provided by sulfur. Therefore, it agrees with what has already been observed in another study where it is explained that theoretically decreasing sulfur element decrease the concentration of charge carriers [17]. The low concentration of carries also reflects a low electrical conductivity and high resistivity; the electrical conductivity is lower than that reported in the literature [4], [18].

The sample CSS 2.29 shows a high concentration of charge carriers and a higher conductivity with reference to the chalcostebite phase. However, the sample presents both phases under study coexisting. This phase combination causes the charge carrier concentration and conductivity to decrease relative to the purest phase observed in the CSS 2.22 sample. This effect has already been described and it is explained that the presence of secondary phases affects the concentration of charge carriers and therefore the conductivity [16]. The CSS 2.22 sample has the highest charge carrier concentration and the highest conductivity in this work. The value of conductivity and charger carrier concentration are similar and even higher than those reported in the literature [4], [9]. Also, this sample is the one with the highest amount of sulfur and the highest percentage of tetrahedrite, which explains its high concentration of charge carriers and its superior electrical properties compared to the other samples. However, the sample presents a secondary phase, which did not affect the electrical properties of the main phase, as in the CSS 2.29 sample.

TABLE III. ELECTRICAL PROPERTIES OF CSS SAMPLES

Sample	Bulk Concentration p (cm^{-3})	Resistivity ρ (Ωcm)	Conductivity σ (1/Ωcm)
CSS 4.00	$2.869x10^{14}$	$4.381x10^{2}$	$3.296x10^{-3}$
CSS 3.20	$6.388x10^{13}$	$2.587x10^{3}$	$4.091x10^{-4}$
CSS 2.29	$2.185x10^{20}$	$1.518x10^{-2}$	$6.588x10^{1}$
CSS 2.22	$3.725x10^{22}$	$1.915x10^{-3}$	$5.223x10^{2}$

E. Seebeck coefficient and power factor

Table IV shows the Seebeck coefficients and power factors of the samples. The CS 4.00 sample has the largest Seebeck coefficient. This may be due to the low concentration of carriers presents. This effect would explain a low thermal conductivity which results in a higher Seebeck coefficient but is necessary quantify this propriety. Although the CSS 4.00 sample has the highest Seebeck coefficient, its low conductivity results in a low power factor. The same effect happens with the CSS 3.20 sample which also presents the $CuSbS_2$ compound in Raman. The CSS 2.29 has a high Seebeck coefficient but a low conductivity, this causes a low power factor as well. The combination of phases produces the low conductivity and the low power factor.

TABLE IV. SEEBECK COEFFICIENT AND POWER FACTOR OF CSS SAMPLES

Sample	Seebeck Coefficient S (μV/K)	Power factor $S^2σ$ (μW/cm·K^2)
CSS 4.00	147.0	$7.12x10^{-5}$
CSS 3.20	55.0	$1.34x10^{-6}$
CSS 2.29	71.7	0.34
CSS 2.22	54.3	1.54

Finally, the CSS 2.22 sample, which presents the tetrahedrite phase in Raman in a higher percentage, presents the highest power factor of 1.54 μW/cm·K^2. This value is lower than that reported in another study for thin films of 2.30 μW/cm·K^2, but this value was obtained at 495 K [9]. In this study, the measurement temperature was around 60 °C (~333 K) which means that values close to those reported by the e-beam technique were obtained [9]. The advantage is that the method reported in this work saves time by no manufacturing a target. In addition, the deposition process is carried out at room temperature and does not require energy consumption to heat the substrate. However, it is necessary to do more experiments varying the thickness of the precursor layers to obtain a stoichiometry close to the ideal.

IV. CONCLUSIONS

Thin films of $CuSbS_2$ and $Cu_{12}Sb_4S_{13}$ phases were obtained by a two-stage process, the sequential deposition of the Sb_2S_3 and CuS layers on glass substrates, followed by annealing at 350 °C in a N_2 atmosphere. To obtain the samples, it was necessary to vary the thickness of the CuS layer and maintain a constant thickness of the Sb_2S_3 layer. It was found that the obtaining of the $CuSbS_2$ and $Cu_{12}Sb_4S_{13}$ phases, when the annealing temperature is kept constant at 350 °C, depends on the thickness of the layers of the precursors. If the thickness of the CuS layer is increased and the Sb_2S_3 is constant, the formation of $Cu_{12}Sb_4S_{13}$ is favored, this due to the presence of high Cu content that allows to obtain the tetrahedrite. Likewise, it was observed that the $Cu_{12}Sb_4S_{13}$ phase has better thermoelectric properties than the $CuSbS_2$ compound, although it was not obtained in pure form. The CSS 2.22 sample presented a greater amount of $Cu_{12}Sb_4S_{13}$ phase with 80 percent; therefore, it was the sample with the best thermoelectric properties. Trough EDS analysis the elemental amount of Cu, Sb, S of the samples was quantified, and it was found that the CSS 2.22 sample is rich in Cu. Also, the band gap of the sample was 1.83 eV. Its charge carries concentration was of $3.725x10^{22}$ cm^{-3} with a p-type conductivity. The conductivity value was $5.223x10^2$ $\Omega^{-1}cm^{-1}$ and the Seebeck coefficient was of 54.3 μV/K. Finally, the power factor value was 1.54 $\mu W/cm{\cdot}K^2$ at 60 °C. According to the results, it can be observed that a competitive thin film was obtained in comparison with others that have been obtained by other techniques; with the advantage that the technique used save time and does not require the manufacture of targets. The purity and stoichiometry of the $Cu_{12}Sb_4S_{13}$ phase could be improved by varying the thicknesses of Sb_2S_3 and CuS layers; as well as modifying the annealing temperature. XRD analysis is required to verify that there are no other micro phases and determine crystal size; as well as the quantification of thermal conductivity to determine the *ZT* values of this sample.

AKNOWLEDGMENT

The authors acknowledgment the support from CONACYT and UAQ provided to the student Daniel Trejo Zamudio for his postgraduate studies. We acknowledge the technical support of Instituto de Energías Renovables, UNAM for the Seebeck coefficient measurements and EDS analysis.

V. REFERENCES

[1] X. Zhang and L. Zhao, "Thermoelectric materials : Energy conversion between heat and electricity," *J. Mater.*, vol. 1, no. 2, pp. 92–105, 2015.

[2] M. Hamid, Elsheikh *et al.*, "A review on thermoelectric renewable energy : Principle parameters that affect their performance," *Renew. Sustain. Energy Rev.*, vol. 30, pp. 337–355, 2014.

[3] Y. F. Wang, K. H. Lee, H. Ohta, and K. Koumoto, "Fabrication and thermoelectric properties of heavil y rare-earth metal-doped $SrO(SrTiO_3)_n$ (n=1,2) ceramics.," *Ceram Int*, vol. 34, pp. 849–52, 2008.

[4] M. I. Medina-Montes *et al.*, "Development of phase-pure $CuSbS_2$ thin films by annealing thermally evaporated CuS/Sb2S_3 stacking layer for solar cell applications," *Mater. Sci. Semicond. Process.*, vol. 80, no. November 2017.

[5] J. Baker *et al.*, "Pressure induced structural transitions in $CuSbS_2$ and $CuSbSe_2$ thermoelectric compounds," *J. Alloys Compd.*, vol. 643, pp. 186–194, 2015.

[6] B. Yang *et al.*, "$CuSbS_2$ as a promising earth-abundant photovoltaic absorber material: a combined theoretical and experimental study," *Chem. Mater.*, vol. 26, pp. 3135–3143, 2014.

[7] A. W. Welch, P. P. Zawadzki, S. Lany, C. A. Wolden, and A. Zakutayev, "Self-regulated growth and tunable properties of $CuSbS_2$ solar absorbers," *Sol. Energy Mater. Sol. Cells*, vol. 132, pp. 499–506, 2015.

[8] S. C. Riha, A. A. Koegel, J. D. Emery, M. J. Pellin, and M. A.B.F., "Low-temperature atomic layer deposition of $CuSbS_2$ for thin-film photovoltaics," *ACS Appl. Mater. Interfaces*, vol. 9, no. 5, pp. 4667–4673, 2017.

[9] D.S. P. Kumar, M. Ren, T. Osipowicz, R. C. Mallik, and P. Malar, "Tetrahedrite ($Cu_{12}Sb_4S_{13}$) thin films for photovoltaic and thermoelectric applications," *Sol. Energy*, vol. 174, no. August, pp. 422–430, 2018.

[10] J. Heo, R. Ravichandran, C. F. Reidy, J. Tate, J. F. Wager, and D. A. Keszler, "Design Meets Nature: Tetrahedrite Solar Absorbers," *Adv. Energy Mater.*, vol. 5, no. 7, p. 1401506, Apr. 2015.

[11] T. Rath, A. J. Maclachlan, M. D. Brown, and S. A. Haque, "Structural , optical and charge generation antimony sulfide thin films prepared from metal," pp. 24155–24162, 2015.

[12] B. Du, R. Zhang, K. Chen, A. Mahajan, and M. J. Reece, "The impact of lone-pair electrons on the lattice thermal conductivity of the thermoelectric compound $CuSbS_2$," *J. Mater. Chem. A*, vol. 5, pp. 3249–3259, 2017.

[13] S. Kharbish, E. Libowitzky, and A. Beran, "Raman spectra of isolated and interconnected pyramidal XS_3 groups (X = Sb, Bi) in stibnite, bismuthinite, kermesite, stephanite and bournonite," no. March, pp. 325–333, 2009.

[14] M. I. Medina-Montes, Z. Montiel-González, N. R. Mathews, and X. Mathew, "The influence of film deposition temperature on the subsequent post-annealing and crystallization of sputtered Sb_2S_3 thin films," *J. Phys. Chem. Solids*, vol. 111, pp. 182–189, Dec. 2017.

[15] L. Wan *et al.*, "Two-stage co-evaporated $CuSbS_2$ thin films for solar cells," *J. Alloys Compd.*, vol. 680, pp. 182–190, 2016.

[16] K. A. Borup *et al.*, "Measuring thermoelectric transport properties of materials," *Energy Enviromental Sci.*, vol. 8, pp. 423–435, 2015.

[17] F. H. Sun *et al.*, "Powder metallurgically synthesized $Cu_{12}Sb_4S_{13}$ tetrahedrites: phase transition and high thermoelectricity," *RSC Adv.*, vol. 7, no. 31, pp. 18909–18916, 2017.

[18] W. Wubet and D.-H. Kuo, "Process limitation for p-type $CuSbS_2$ semiconductor with high electrical mobility of $20cm^2\ V^{-1}\ s^{-1}$," *Mater. Res. Bull.*, vol. 53, pp. 290–294, May 2014.